Kinetic process of UV Cu^+ laser in Ne-CuBr longitudinal pulsed discharge

Pan Bai-liang, Chen Gang, Mao Bang-Ning, and Yao Zhi-Xin

Department of Physics, Zhejiang University, 310027, Hangzhou, P. R. China
pbl66@zju.edu.cn

Abstract: The kinetic process of Cu^+ UV laser in Ne-CuBr longitudinal pulsed discharge is analyzed and a comprehensive self-consistent physical model is developed. The temporal evolutions of discharge parameters, main particle densities, the electron temperature, and the laser pulse intensity are numerically calculated. The model results illustrate the process of population inversion and the lasing mechanism. The calculations on the influences of the tube radius and Br atoms on the laser output characteristic well explain the experimental results.

OCIS codes: (140.0140) Lasers and laser optics; (140.7240) UV, XUV, and X-ray lasers; (140.3210) Ion lasers; (140.3430) Laser theory.

References and Links

1. J. R. McNeil, G. J. Collins, K. B. Persson, and D. L. Franzen, "Ultraviolet laser action from Cu II in the 2500-A region," Appl. Phys. Lett. **28**, 207-209 (1976).
2. K. G. Hernqvist, "Continuous laser oscillation at 2703 A in copper ion," IEEE J. Quantum Electron. **13**, 929–934 (1977).
3. R. Solanki, W. M. Fairbank Jr., and G. J. Collins, "Multiwatt operation of Cu II and Ag II hollow cathode lasers," IEEE J. Quantum Electron. **16**, 1292-1294 (1980).
4. B. Auschwitz, H. J. Eichler, and W.Wittwer, "Extension of the operating period of an UV Cu II laser by admixture of argon," Appl. Phys. Lett. **36**, 804-805 (1980).
5. K. Jain, "New UV and IR transitions in gold, copper, and cadmium hollow cathode lasers," IEEE J. Quantum Electron. **16**, 387-388 (1980).
6. Z. Donko, L. Szalai, K. Rozsa, M. Ulbel, and M. Pockl, "High-gain ultraviolet Cu-II laser in a segmented hollow cathode discharge," IEEE J. Quantum Electron. **34**, 47–52 (1998).
7. N. K. Vuchkov, K. A. Temelkov, and N. V. Sabotinov, "UV lasing on Cu in Ne–CuBr pulse longitudinal discharge," IEEE J. Quantum Electron. **35**, 1799-1804 (1999).
8. C. E. Little and N. V. Sabotinov, *Pulsed Metal Vapor Lasers*, 113–124 (C. E. Little and N. V. Sabotinov, Kluwer, Netherlands, 1996).
9. N. K. Vuchkov, K. A. Temelkov, P. V. Zahariev, and N. V. Sabotinov, "Influence of the Active Zone Diameter on the UV-Ion Ne–CuBr Laser Performance," IEEE J. Quantum Electron. **37**, 1538-1546 (2001).
10. N. K.Vuchkov, K. A.Temelkov, P. V.Zahariev, and N. V. Sabotinov, "Kinetic and experimental study on the influence of the inside tube diameter on the UV ion Ne-CuBr laser output parameters," in *International Conference on Atomic and Molecular Pulsed Lasers IV*, V. F. Tarasenko, G. V. Mayer, and G. G. Petrash, eds., Proc. SPIE **4747,** 156-163 (2002).
11. N. K. Vuchkov, K. A. Temelkov, P. V. Zahariev, and N. V. Sabotinov, "Output parameters and a spectral study of UV Cu^+ Ne–CuBr laser," Opt. & Laser Technology **36**, 19-25 (2004).
12. N. K. Vuchkov, K. A. Temelkov, and N. V. Sabotinov, "Effect of hydrogen on the average output power of the UV Cu^+ Ne-CuBr laser, " IEEE J. Quantum Electron. **41**, 62-65 (2005).
13. M. J. Kushner, "A self-consistent model for high-repetition rate copper vapor laser," IEEE J. Quantum Electron. **17**, 1761-1764 (1981).
14. R.J. Carman, "A self-consistent model for a longitudinal discharge excited He-Sr recombination laser," IEEE J. Quantum Electron. **26,** 1588-1607 (1990).

#72809 - $15.00 USD Received 12 July 2006; revised 21 August 2006; accepted 27 August 2006

15. R. J. Carman, J. W. Brown, and J. A. Piper, "A self-consistent model for the discharge kinetics in a high-repetition-rate copper-vapor laser," IEEE J. Quantum Electron. **30**, 1876–1894 (1994).
16. Jin Y, Pan B L, Chen G, Chen K, and Yao Z X, "Numerical study on the terminating mechanisms of copper vapor laser pulse," Acta Phys. Sin. (in Chinese) **53,** 1799-1803 (2004).
17. Bai-Liang Pan, Gang Chen, Xing Chen, and Zhi-Xin Yao, "Numerical and experimental investigation on self-terminating and recombination lasers in univalent ions of calcium and strontium," J. Appl. Phys. **96**, 34-39 (2004).
18. R. J. Carman, R. P. Mildren, M. J. Withford, Daniel J. W. Brown, and J. A. Piper, "Modeling the Plasma Kinetics in a Kinetically Enhanced Copper Vapor Laser Utilizing HCl + H_2 Admixtures," IEEE J. Quantum Electron. **36,** 438-449 (2000).
19. Chen Gang, Pan Bai-liang, Chen Kun, and Yao Zhi-xin, "A novel excitation circuit used for CuBr lasers," J. Optoelectronics Laser (in Chinese) **14,** 1142-1145 (2003).
20. T. Holstein, "Imprisonment of radiation in gases II," Phys. Rev. **83**, 1159–1168 (1951).

1. Introduction

Lately, there has been sustained interest in the longitudinal pulsed discharge Cu^+ ultraviolet (UV) lasers, particularly in the 248.6nm line, which is very close to the 248.5nm laser line of the KrF excimer laser. The UV Cu^+ laser with 1W order average power can be used in microelectronics, microbiology and genetic engineering. Although the UV Cu^+ laser in a hollow cathode discharge (HD) was firstly reported in 1976 [1], and eight Cu^+ laser lines were obtained in the 248.6-270.3-nm spectral range in HD [2-5], this kind of laser has disadvantages of instability of discharge, serious cathode erosion, short lifetime of several hours [6], and lower output power. So it is hard to develop a practical laser device for real applications. An important progress was made for the first time when laser oscillation was obtained on four Cu^+ lines, 248.6 nm, 252.9 nm, 260.0 nm, and 270.8 nm in Ne-CuBr with a nanosecond pulsed longitudinal discharge [7]. This discharge tube is the same as the steadily operated CuBr laser, which has the long lifetime about 1000 hours and high output power [8]. Based on the similar technical method, it is promising to develop a long lifetime and high power Cu^+ UV laser in Ne-CuBr longitudinal discharge. Therefore, in recent years, many investigations have been conducted on the Cu^+ UV lasers [9-12]. On the other hand, due to the very low gain of UV Cu^+ laser medium, compared to the visible 578.2nm and 510.6nm of the atomic copper laser, the refined experimental conditions are needed to obtain laser oscillation. Although many experimental attempts have been made to improve the output characteristic of Cu^+ UV laser in Ne-CuBr discharge, the comprehensive computer model for the Cu^+ UV laser, as an integral part of experiment and theory hasn't been developed up to now. There for, it is necessary to establish a computer model to study the kinetic process of this laser in order to provide the detailed information of the mechanism and operation parameters to the experiment.

Computer model has been used to simulate the temporal behaviors of the microscopic parameters, and provide the detailed information on kinetic processes in the discharge plasma where experimental techniques cannot be used [13-17]. The model of self-terminating copper and copper halide vapor laser has been well developed [15, 16, 18], and the results predicted by the model agree well with the experiment. Based on our previous model on copper vapor laser [16], this paper describes a self-consistent model to simulate the kinetic behavior of UV Cu^+ laser in Ne-CuBr pulsed longitudinal discharge.

A description of the model, including the external excitation circuit, main particle species, the electron temperature, and the intracavity laser intensity is given in Section 2. In Section 3, the results predicted by the model are compared with the experimental data and discussed in detail. A summary of the results is given in Section 4.

#72809 - $15.00 USD Received 12 July 2006; revised 21 August 2006; accepted 27 August 2006

2. Description of the model

The model consists of an excitation circuit and a comprehensive description of the UV laser kinetics in Ne-CuBr discharge plasma. We choose the interactive circuit (IC) as the discharge excitation circuit [7, 19], which has the characteristics of compressing the width of the discharge current pulse and improving the current rising rate. The assumption that the discharge tube is longitudinally homogeneous with respect to all particle densities was used, and Maxwellian distribution was used to describe the electron energy distribution function (EEDF) in calculating the rate coefficient according to the impact cross section.

The partial Cu, Cu^+ energy levels and corresponding laser radiation, together with Ne atom energy level are shown in Fig. 1(a) and Fig. 1(b). Eleven copper atomic energy levels and ten ionic levels were considered in the model. From the ionic energy levels, one can see that the upper laser level $5s^3D_1$ lies closely to the Ne^+ ground state with a small energy difference (~ 0.2eV), so it can be easily populated

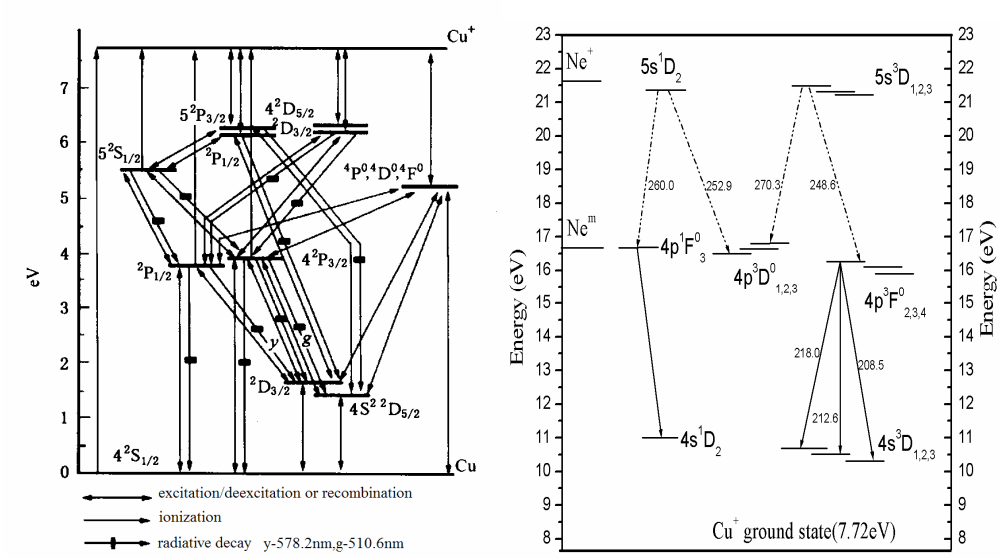

Fig. 1. (a). Schematic diagram of Cu atom energy levels. (b). Schematic diagram of Cu^+ and Ne energy levels

via charge exchange reaction between Cu and Ne^+ ground states (Eq. (1)). Analogously, the lower laser levels 4p states can be populated via penning collisions between neon metastable level Ne^m and copper ground state Cu_0 because of the close energy level (Eq. (2)). Meanwhile, these levels can be mainly depopulated by UV spontaneous emission to the 4s Cu^+ metastable levels (Cu^{+m}) with fast transition probability.

$$Ne^+ + Cu_0 \rightarrow (Cu^+)^*(5s) + Ne + \Delta E\,. \tag{1}$$

$$Ne^M + Cu_0 \rightarrow Ne + (Cu^+)^*(4p) \tag{2}$$

Three neon levels are included: the ground-state Ne, metastable state Ne^m, and ion ground-state Ne^+. The kinetic process of laser oscillation is focused on the 248.6nm in this model for economy. Accordingly, the varying rate equations of the species populations are given below.

#72809 - $15.00 USD Received 12 July 2006; revised 21 August 2006; accepted 27 August 2006

2.1 Copper atoms

$$\frac{dCu^*}{dt} = \kappa_i \cdot Cu \cdot n_e - \kappa_k \cdot Cu^* \cdot n_e - \gamma_i \cdot Cu^* \cdot n_e + \alpha_k \cdot Cu^+ \cdot n_e{}^2 \pm A_i \cdot Cu^* \pm I_p \cdot \gamma_0 \cdot / h\nu - \nabla \cdot \bar{\Gamma}. \quad (3)$$

2.2 Copper ions

$$\frac{dCu^+}{dt} = \kappa_i \cdot Cu \cdot n_e + \sum_i \kappa_i \cdot Cu^* \cdot n_e + \sum_k \gamma_k \cdot Cu^{+*} \cdot n_e - \alpha_i \cdot Cu^+ \cdot n_e{}^2 - \nabla \cdot \bar{\Gamma}. \quad (4)$$

$$\frac{dCu^{+m}}{dt} = \kappa \cdot Cu^+ \cdot n_e + \sum_k \gamma_k \cdot (Cu^+)_k \cdot n_e + \sum_i A_{i1} \cdot (Cu^+)_i + Kp_1 \cdot Ne^m \cdot Cu - \sum_k k_k \cdot Cu^{+m} \cdot n_e - \gamma \cdot Cu^{+m} \cdot n_e - \nabla \cdot \bar{\Gamma}. \quad (5)$$

$$\frac{dCu^{+l}}{dt} = Kp_2 \cdot Ne^m \cdot Cu + \sum_i k_i \cdot (Cu^+)_i \cdot n_e + \sum_k \gamma_k \cdot (Cu^+)_k \cdot n_e + \sum_i A_{i2} \cdot (Cu^+)_i - \sum_k k_k \cdot Cu^{+l} \cdot n_e - \sum_i \gamma_i \cdot Cu^{+l} \cdot n_e + B \cdot I_p \cdot \Delta N - \sum_i A_{2i} \cdot Cu^{+l} - \nabla \cdot \bar{\Gamma}. \quad (6)$$

$$\frac{dCu^{+u}}{dt} = K_{CT} \cdot Ne^+ \cdot Cu + \sum_i k_i \cdot (Cu^+)_i \cdot n_e + \sum_k \gamma_k \cdot (Cu^+)_k \cdot n_e - \sum_i A_{3i} \cdot Cu^{+u} - \sum_k k_k \cdot Cu^{+u} \cdot n_e - \sum_i \gamma_i \cdot Cu^{+u} \cdot n_e - B \cdot I_p \cdot \Delta N - \nabla \cdot \bar{\Gamma}. \quad (7)$$

where Cu^{+m}, Cu^{+l}, Cu^{+u} are the population densities of the Cu^+ metastable level(4s), the lower ($4p\ ^3F^o_2$) and the upper ($5s\ ^3D_1$) laser levels of 248.6nm, respectively. The electron density n_e is inferred from the sum of the local ion densities assuming that the degree of ionization and space-charge fields are sufficiently high to ensure charge neutrality throughout the bulk of the gas.

The subscripts *i* and *k* refer to processes involving lower and higher energy levels in relation to the energy level of a given species, κ and γ are the respective rate coefficients for excitation (or ionization) and deexcitation, α is the recombination coefficient, A_i is the corresponding transition probability for radiative decay, and Kp_1, Kp_2 are the rate coefficients for Penning collisions. The first term in Eq. (5) represents the charge exchange reaction between Ne^+ and Cu atom ground state with the rate coefficient K_{CT}. Stimulated emission process of 248.6nm laser line is represented in the Eqs. (6) and (7) with the coefficient *B*, where I_p is the intracavity photon flux. Particle diffusion is represented throughout by the divergence of the radial particle flux Γ.

#72809 - $15.00 USD Received 12 July 2006; revised 21 August 2006; accepted 27 August 2006

2.3 Intracavity laser photon flux I_p

The continuity equation for the photon flux at 248.6 nm is given by

$$\frac{dI_p}{dt} = cI_p\gamma_0 L_0 / L_c + I_p c \ln\left(R_1 R_2\right)/\left(2L_c\right) + A_1 Cu^{+u} h\nu c d\Omega/\left(4\pi\right). \qquad (8)$$

Where R_1 and R_2 are the cavity mirror reflectivities, c is the speed of light, and L_c is the cavity length. The first term represents stimulated emission or absorption in the plasma with gain γ_0, the second term gives the losses at cavity mirrors, and the third term denotes the spontaneous emission from which the laser field builds up, where A_1 is the transition probability from the transition at 248.6 nm and $d\Omega/4\pi$ is the solid angle.

2.4 Energy conservation

The equation used to solve the electron temperature is given by

$$\frac{d\left(1.5 n_e K_b T_e\right)}{dt} = \frac{n_e e^2 E^2}{m_e \nu_t} + \sum_{ij} \gamma_{ij} n_e N_j \varepsilon_{ij} + \sum_j \eta_p Cu N_j \varepsilon_p + \sum_{ij} \beta_m Ne_i^* Ne_j^* \varepsilon_m$$

$$-2m_e \sum_j \left(\nu_j / m_j\right) \cdot 1.5 n_e k_b \left(T_e - T_0\right) - \sum_{ij} \kappa_{ij} N_i n_e \varepsilon_{ij} . \qquad (9)$$

The first term is for the energy gained from the longitudinal electric field E, the second term represents heating of electron gas by superelastic collisions, and the third term takes into account heating by fast electrons liberated in Penning collisions, and the fourth term refers to heating via helium metastable-mestastable ionizing collisions whereby a fast electron is liberated with energy ε_m, and the fifth term represents energy loss due to elastic collisions with the neutral-ions gas, while the sixth term denotes the energy losses associated with inelastic electron collisions with atoms or ionic species.

Equations (3)-(9) and the equation of electron density as well as circuit equations given in [19] and Cu atom rate equations described in [16] constitute a set of coupled first-order differential equations of the model. The standard initial conditions used in this model (Table 1) such as neon pressure, charge voltage, circuit parameters, and the density of ground state copper atoms are the same as those from a recent experimental study [9]. The model of 56 first-order coupled ordinary differential equations is solved by the method of Backward Differentiation Formula (BDF). A set of initial conditions is chosen to begin the calculation after calculating for 10 excitation-afterglow cycles to reach the condition of temporal self-consistency. The rate coefficients used in the model are cited from [13-18]. Thus, the lasing process parameters including population densities, the discharge current, the lasing pulse, the electron density, and the electron temperature can be acquired.

#72809 - $15.00 USD Received 12 July 2006; revised 21 August 2006; accepted 27 August 2006

Table 1. Standard Initial Conditions

Plasma column length L_0/cm	86
Optical cavity length Lc/cm	180
Mirror reflectivity R_1/R_2	0.04/1.0
Tube diameter R_T/cm	1.2
Ne pressure P_{Ne}/kPa	**1.7**
Wall temperature T_w/K	694
Capacitance bank $C_1/ C_2 /C_3 /C_4$	0.5nF/0.235nF/0. 235nF/2.2nF
Charging voltage U_{C1}/U_{C2}	10kV/10kV
Circuit inductance $L/L_1/L_2/L_R$	2μH/0.25μH /0.25μH /0.5μH
Pulse repetition frequency f/kHz	20

3. Simulation results and discussion

3.1 Discharge current pulse and electron temperature

The discharge current pulses of calculation and experiment are shown in Fig. 2. The raise ratio of the front edge and the magnitude of current pulse mainly influence the electron temperature *Te* in the excitation period. As can be seen, the model result agrees well with the experiment, and the accuracy of current pulse can give an accuracy value of *Te* [15, 16]. The difference of current back edge comes from the complex plasma resistance expression due to the large number of particles after the excitation

#72809 - $15.00 USD Received 12 July 2006; revised 21 August 2006; accepted 27 August 2006

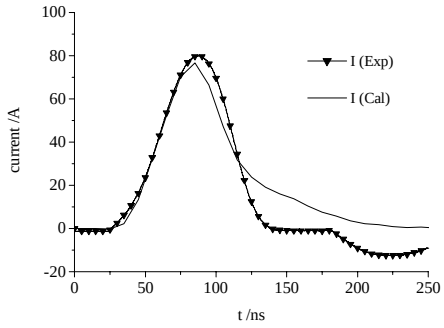

Fig. 2. Discharge current I of the laser tube

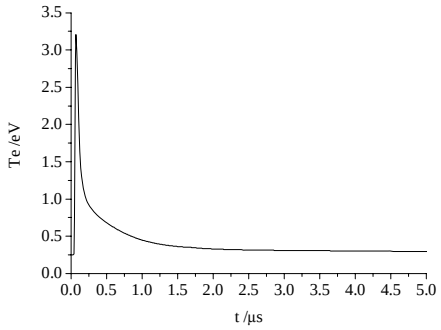

Fig. 3. Evolution of the electron temperature

pulse, but it rarely influences the maximum of the electron temperature *Te*, and the difference will disappear in the afterglow. Figure 3 gives the evolution of the electron temperature *Te*. Here, the maximum value of *Te* reaches about 3.2eV in the excitation pulse, which is slightly lower than those in Ne-Cu discharge plasma [15] because of the existence of vast Br atoms and ions.

3.2 Kinetic process of UV Cu^+ laser

During the early discharge pulse, the current pulse *I* and the electron temperature *Te* all reach its maximum, and neon and *Cu* atoms are rapidly ionized predominantly by stepwise electron collisions via the excited states. So the electron density and all ions reach a max value in the excitation pulse. With the end of the discharge, *Te* begins to decrease quickly and the deexcitation and recombination processes will predominantly occur, as a result, the densities of all particles have a decreasing process in the afterglow pulse. Figure 4 represents the calculated temporal behavior of the major ions and the electron density at tube center in the discharge period. It is emphasized that the density of Ne^+ decreases evidently faster than other ions in the afterglow. This difference mainly attributes to the charge exchange reaction between Ne^+ and the Cu ground state, which has the higher density in the afterglow. As has

#72809 - $15.00 USD Received 12 July 2006; revised 21 August 2006; accepted 27 August 2006

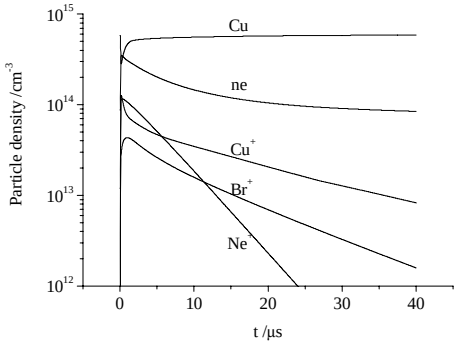

Fig. 4. Temporal evolutions of population densities of main ions and electron on the tube axis.

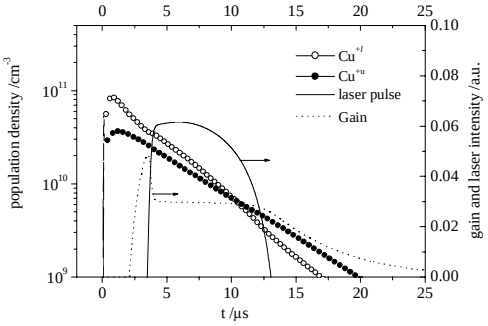

Fig. 5. Temporal evolutions of $Cu^{+u}$and Cu^{+l} population

been described above, the upper laser level of 248.6nm is pumped mainly by the charge exchange reaction between Ne^{+} and Cu ground state in the discharge afterglow. As shown in Fig. 3 and Fig. 4, about 1μs later after the excitation pulse, the electron temperature has fallen to about 0.3-0.5eV, the excited state copper species begin to deexcitation and the copper ground state begin to rise to its initial density. With the increase of copper ground state, together with the sufficient high density of Ne^{+} and Neon metastable level Ne^{m}, the upper and the lower laser levels begin to be populated via the charge exchange reaction and Penning collision excitation in afterglow. Such as shown in Fig. 5, the upper and the lower laser levels reach a maximum density at about 1μs, and then begin to decay due to the spontaneous emission. Until about 3.5μs, the gain coefficient and the relative inversion reach maximum value and the laser pulse occurs. Between 3.5-13μs, the gain coefficient and inversion density hold on a steady value, as a result, the laser pulse duration can last about 10 μs. These modeling results agreed well with the experimental observation in [9]. With the depletion of Ne^{+} due to charge exchange reaction, the laser pulse intensity begins to decrease till disappear.

3.3 Depopulation of the lower laser level

The lower laser level can be pumped by electron impact in early discharge pulse and by Penning collision via Ne^{m} in the afterglow. While the depopulation process of the lower level is mainly through the UV spontaneous emission to the Cu^{+} metastable levels Cu^{+m}. Although this process is an efficient way to the deexcitation of lower laser level, the high density of Cu^{+m} in the afterglow will lead to a remarkable radiative trapping effect between the lower laser level and Cu^{+m} levels, which will increase the density of the lower laser level. As a result, the density of inversion population and the laser output power will decrease significantly. Only if the radiative trapping effect is quenched or destroyed effectively, both the laser output power and efficiency can be improved. A theoretical analysis on how to restrain the radiative trapping effect is given below.

According to Holstein's theory [20], in a cylinder of plasma of radius *R*, the effective transition probability A_{eff} can be written by

$$A_{eff} = 1.6A\left[(k_0R+\phi)\left[\pi\ln(k_0R+\phi)\right]^{1/2}\right]^{-1} \quad (\ k_0R>3\ ), \qquad (10)$$

#72809 - $15.00 USD Received 12 July 2006; revised 21 August 2006; accepted 27 August 2006

$$A_{eff} = A\exp(-0.653[k_0 R]^{0.81}) \qquad (k_0 R < 3). \quad (11)$$

Where k_0 is the absorption coefficient at line center. As discussed in [9], A_{eff} is strongly affected by the radius R of laser tube. In this case, the depopulation of lower laser level is mainly through UV spontaneous emission with the coefficient A_{eff}, so the laser output characteristic is influenced strongly by the laser tube radius. Figure 6 shows the dependence of the photon (corresponding to the laser output power) and Cu^{+m} densities on different radius R. As can be seen, the maximum photon density almost doubled when the radius decreased from 8mm to 6mm. It also shows that the laser pulse delay decreased from 2μs to 1.5μs, although at which time the density of Cu^{+m} increased about 50% from 5×10^{12} to 7.5×10^{12}. These varieties in microcosmic parameters clearly show that the negative influence of radiative trapping on depopulating the lower laser level was effectively restrained with the diameter reduction. All these results of the model and the experiment in [9] show that the delay of the laser pulse will be shortened, and the laser output characteristic will be improved well with the decrease of tube radius R.

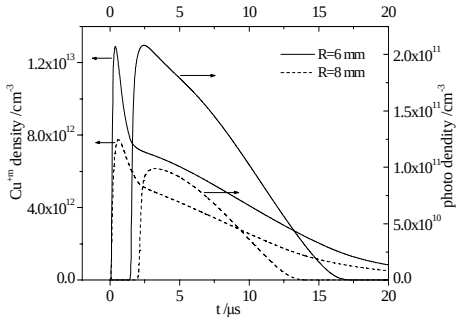

Fig. 6. Influence of the tube radius R on Cu^{+m} density and the laser output characteristic

3.4 Influence of Br on the laser output characteristic

The copper atoms in CuBr Cu^+ UV laser are produced mainly by electron impact dissociation of the CuBr molecules during the discharge period. In the high repetition frequency discharging, CuBr vapor is almost fully dissociated and hardly recombined in one discharge cycle due to its longer recombination time. Br atoms would reduce the maximum value of electron temperature Te ($\sim$ 3.5eV) in the Ne-CuBr plasma, compared to 6eV in the Ne-Cu plasma. However, the existence of Br atoms has the advantage of enhancing laser output power for UV Cu^+ laser due to its own mechanism. As seen in [9], four Br^+ levels are located closely to the Cu^+ metastable levels. These levels can be populated mainly by Penning collision with neon metastable levels Ne^m due to the high excitation energy. A preferential condition is that the rate constant for Penning ionization of Br^+ is about ten times as large as that of the lower laser and metastable Cu^+ levels [9]. As a result, this process leads to the reduction of Ne^m and Cu^{+m} densities and the increase of laser power.

#72809 - $15.00 USD Received 12 July 2006; revised 21 August 2006; accepted 27 August 2006

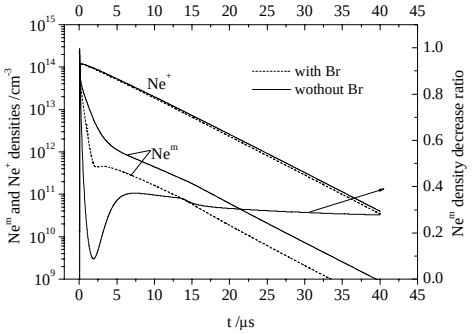

Fig. 7. Influence of Br on Ne^m and Ne^+ densities

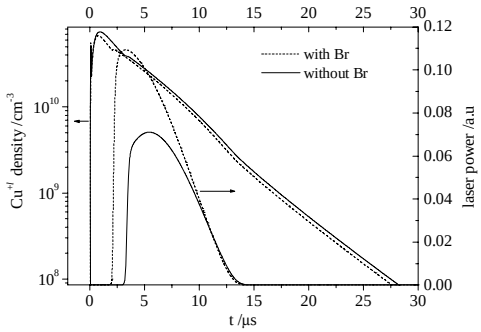

Fig. 8. Influence of Br on Cu^{+l} density and the laser power

Figure 7 represents the modeling results of the influences of Br atoms on neon metastable and neon singly charged ion densities. One can see from Fig.7, the process of Penning ionization of Br^+ can strongly decrease the Ne metastable density in the discharge afterglow, while the density of Ne^+ scarcely changes due to the affection of Br. The reduction of Ne^m decreases slightly the density of lower laser level Cu^{+l}, which is mainly pumped by Penning collision between Ne^m and Cu ground state. As a result, the inversion population density increases evidently and the laser power has a marked enhancement by about 50%, such as shown in Fig. 8.

4. Conclusion

Based on the physical mechanism of Cu^+ UV laser, a self-consistent computer model was developed to simulate the discharge kinetics and Cu^+ UV lasing characteristic in Ne-CuBr longitudinal pulsed discharge. The temporal evolution of population densities of main particles in Ne-CuBr discharge plasma was calculated. The model results agreed well with the experimental data by comparing the electrical I-V characteristic of discharge tube. The excitation mechanism of the upper laser level and the lasing process were clearly predicted by the calculation. It was shown that the charge exchange reaction between Cu ground state and Ne^+ was the dominant mechanism for the excitation of the upper laser level. When Helium was used as buffer gas in experiment, Cu^+ UV laser cannot be obtained [8]. Due to the marked negative influence of radiative trapping on depopulating the lower laser level, the laser output power will increase with the reduction of tube radius. Model results also predicted the influence of tube diameter on the restraint of radiative trapping, and explained clearly the enhanced effect of Br atoms on the laser output power observed in [9]. Thus, the model can provide an effective way to improve the Cu^+ UV laser output characteristic in experiment.

Acknowledgments

This work was supported by the National Natural Science Foundation of China (Grant Nos. 10374081, 10574111), the Inertial Confinement Fusion Research Foundation (Grant No. 2004AA84TS04), and China Postdoctoral Science Foundation (Grant No. 2004036482).

#72809 - $15.00 USD Received 12 July 2006; revised 21 August 2006; accepted 27 August 2006